Shifting of the absorption edge in TiB_2/TiB(N)/Si_3N_4 solar selective coating for enhanced photothermal conversion

Atasi Dan [a], Kamanio Chattopadhyay [b, c], Harish C. Barshilia [d, *], Bikramjit Basu [a, b, *]

[a] Materials Research Centre, Indian Institute of Science, Bangalore 560 012, India

[b] Interdisciplinary Centre for Energy Research, Indian Institute of Science, Bangalore 560 012, India

[c] Materials Engineering, Indian Institute of Science, Bangalore 560 012, India

[d] Nanomaterials Research Laboratory, Surface Engineering Division, CSIR-National Aerospace Laboratories, Bangalore 560 017, India

Abstract

The concentrated solar power systems for solar energy applications demand the development of spectrally selective absorber coating with high selectivity. This is possible by careful compositional selection of absorber thin films with an aim to shift the optical absorption edge towards higher wavelength side. In this context, the present work aims at developing such a coating, based on TiB_2/TiB(N)/Si_3N_4 by tailoring magnetron sputtering parameters. This multilayer exhibits a high absorptance of 0.964 and a moderately low emittance of 0.18 at 82 °C. The attainment of excellent spectral selectivity. This spectral selectivity has been explained in terms of systematic variation or gradient in refractive index and extinction co-efficient throughout the multilayer stack.

Keywords: Spectrally selective absorber, Magnetron sputtering, Thin films, Spectroscopic ellipsometry

[*]Corresponding Authors:

Email: harish@nal.res.in (Harish C. Barshilia);

bikram@iisc.ac.in (Bikramjit Basu)

1. Introduction

The solar thermal power systems have a strong potential to emerge as a leading technology in contributing significantly to world's energy supply (Duffie and Beckman, 2013; Gauché et al., 2017; Thirugnanasambandam et al., 2010). These systems require solar collectors to convert significant amount of solar energy into thermal energy (Kalogirou et al., 2016). Solar collectors consist of spectrally selective solar absorber coatings, which should maximize the efficiency of the photothermal systems by absorbing maximum amount ($\alpha \geq 0.95$) of solar radiation with minimizing thermal heat loss ($\varepsilon \leq 0.05$) (Dan et al., 2017; Granqvist and Niklasson, 2018; Selvakumar and Barshilia, 2012). The selective performance of a material can be achieved by introducing a sharp discontinuity of the reflectance around absorption edge (Selvakumar et al., 2014). The tuning of optical properties in line with this specific requirement demands careful selection of materials in the absorber thin film.

The structures include intrinsic absorbers (Chen and Boström, 2016), semiconductor-metal tandems (Jeong et al., 2017), multilayer stacks (Dan et al., 2016a), cermets (Klochko et al., 2015), textured absorbers (Gupta et al., 2018) , etc. In recent years, the design of several multilayer architectures (WAlN/WAlON/Al_2O_3 (Dan et al., 2016b, c), ZrO_x/ZrC-ZrN/Zr (Usmani and Dixit, 2016), $TiAlN_x$/$TiAlN_y$/Al_2O_3 (Soum-Glaude et al., 2017), CrTiAlN/TiAlN/AlSiN (Valleti et al., 2014), TiAlN/TiAlON/Si_3N_4 (Barshilia et al., 2006), CrAlN/CrAlON/Al_2O_3 (Zou et al., 2015), Al_2O_3(L)-WC/Al_2O_3(H)-WC/Al_2O_3 (Gao et al., 2016), $MoSi_2$-Si_3N_4/Si_3N_4/Al_2O_3 (Rodríguez-Palomo et al., 2018)) has been extensively investigated as these structures allow multiple reflections at the interfaces of different layers to enhance the absorption in solar radiation wavelength range, while maintaining a low thermal emittance.

However, an extensive literature survey reveals that spectrally selective properties of TiB_2 -based multilayer thin film has not yet been investigated. The above-mentioned studies indicate that various absorber thin films have emerged over the years and it was found that multilayer spectrally selective absorbers are very sensitive to the composition of individual layer. For capturing significant amount of solar radiation, the metallic property and refractive index of each layer should decrease from substrate to surface in a typical multilayer absorber. Considering the conductive property of TiB_2, it can be featured as the first layer of the selective coating. On the other hand, dielectric Si_3N_4 has emerged as one of the most promising anti-reflecting layer, an essential part of optically selective films (Feng et al., 2015; Kim et al., 2013). Moreover, the incorporation of N_2 may lower the refractive index of TiB(N) than TiB_2 and also lead to an intermediate property between conducting TiB_2 (high refractive index) and insulating Si_3N_4 (low refractive index).

Apart from material selection, the choice of processing strategy is equally important. Worldwide, advanced deposition technologies, such as, electrodeposition, chemical vapour deposition, sputtering and allied techniques have been utilized to fabricate such selective coatings using multiple material systems. For last two decades, the fabrication of spectrally selective absorbers using sputtering has been appreciated from an industrial perspective. However, the deposition during sputtering is a complex process. In the present study, we have primarily varied target power, deposition time and the gas flow rate to study their influence on the selective optical performance of thin film. The sputtering parameters for the present deposition process is listed in Table 1. Our main aim was to develop a multilayer thin film with a graded refractive index profile which will exhibit enhanced absorption at a wider window of solar wavelength and reduced emittance in infrared range.

In the above backdrop, we have investigated the possibility of designing a novel TiB_2/TiB(N)/Si_3N_4 –based graded absorber coating for photothermal systems. Attempts have

been made to explore deposition conditions for achieving spectral selectivity. The underlying physical mechanisms of high absorption of solar radiation and low thermal emittance have also been discussed.

2. Experimental

2.1. Deposition of the coating

$TiB_2/TiB(N)/Si_3N_4$ films were deposited on stainless steel (SS) substrates (35 mm × 35 mm × 2 mm) by DC and RF magnetron sputtering of highly pure (> 99.99%) TiB_2 and Si targets (diameter = 0.076 m). Prior to deposition, the substrates were metallographically polished and chemically cleaned. The base pressure of the vacuum chamber was pumped down to 5.0×10^{-4} Pa. The vacuum system was equipped with a rotary and a turbomolecular pump. The gas flow rates inside the chamber were controlled by standard mass flow controllers. The TiB_2 layer was developed in Ar plasma, while deposition of TiB(N) and Si_3N_4 layers was performed in Ar + N_2 environment. The Ar gas flow rate was kept constant at 20 sccm for all layers. The N_2 gas flow rate was 1 and 2 sccm for TiB(N) and Si_3N_4 layers, respectively. Sputtering of the optimized thin film was carried out at a power density of 1.65 W/Cm^2. All the layers were deposited at a substrate temperature of ~ 40 °C. The structure of the coating has been presented in Fig. 1.

2.2.Characterization of the coating

The total hemispherical absorptance (α) and emittance (ε) of the coatings were measured using solar spectrum reflectometer (Model SSR) and emissometer (Model AE) of M/s. Devices and Services, the details of which can be found elsewhere (Selvakumar et al., 2010). The solar reflectometer was calibrated using air mass 2. The emittance was measured at 82 °C. It is important to mention that the emissometer is a special kind of instrument, which is usually operated to evaluate the emittance of solar absorber coatings developed for flat plate

thermal collector having maximum working temperature of 80-90 °C (Saleh and Mosa, 2014; Wallner et al., 2008). The absorptance and the emittance values were evaluated at four different positions. The averages of these values are reported in the preset paper. While offering a resolution up to 0.001, the solar spectrum reflectometer ensures the accuracy of measured absorptance values within ± 2%. The reproducibility of the emittance values measured by the emissometer is ± 0.01 emittance units.

The spectral response of the absorber was recorded using UV-Vis–NIR spectrophotometer (PerkinElmer Lambda 950) in solar wavelength range (0.3-2.5 μm), with an illumination spot size of 5 mm × 5 mm. The spectrophotometer was equipped with a 150 mm integrating sphere to measure total reflectance. FTIR spectrometer (PerkinElmer Frontier) with an integrating sphere attachment was used to collect the reflectance spectra of the sample in the operating range of 2.5-25 μm. Transmission electron microscopy (FEI Tecnai T20 U-TWIN TEM) was carried out on the cross-sectional samples prepared using the UHR dual beam focused ion beam system (FIB, Helios NanoLab 600i, FEI). The coatings were characterized by a VASE spectroscopic ellipsometer (SE) M-2000 (JA Woolam Co, Inc, USA) in the spectral range 200-1000 nm. The analysis of acquired data was performed using completeEASE software, supplied with the ellipsometer.

3. Results

The spectrally selective properties of thin films are strongly dependent on the deposition parameters. It has been observed that a slight change in the sputtering environment can significantly influence the optical properties. Hence, we have tried to find how the spectral performance of TiB_2/TiB(N)/Si_3N_4 thin film is controlled by deposition parameters. A brief discussion of the strategy that has been followed will now be presented.

3.1. Reactive sputtering conditions

3.1.1. Influence of sputtering power and deposition time on TiB_2 layer

In the optimization process, the first aim was to achieve the highest possible absorptance of first layer, i.e., TiB_2. In order to reach the goal, the efforts were made in selecting the sputtering power of TiB_2 target. The low limit must maintain the DC glow discharge in the abnormal discharge regime, which is the operative domain for sputtering power. Fig. 2 (a) represents the reflectance spectra of four different TiB_2 coatings, deposited at 50, 75, 100 and 150 W, respectively, keeping deposition time constant at 3 min. The coating deposited at 150 W exhibits high reflectance in the wavelength range of ~ 400-2500 nm, which results in a low absorptance in solar spectrum. On the other hand, the coating fabricated at 75 W possess < 14% reflectance from 415 to 775 nm, i.e., the most intense part in the solar radiation, which gives rise to a high absorptance. The absorption edges shift to higher wavelength for the films prepared with different TiB_2 target powers. The absorption edge can be observed at ~ 414, 566 and 840 nm for target powers of 50, 75 and 100 W, respectively (see Fig. 2(b)). The absorption edge disappears on further increase of target power to 150 W. The absorptance and emittance values of the SS/TiB_2 coating as a function of target power have been shown in Fig. 2(c). The data clearly exhibit that absorptance is maximum for the coating fabricated at 75 W and subsequently decreases with an increase in target power. The emittance, on the other hand, is constant at 0.12 till a power of 100 W. However, it increases rapidly on further increase in target power till 150 W. Hence, the target power for SS/TiB_2 coating was optimized at 75 W to achieve an absorptance and emittance of 0.798 and 0.14, respectively.

We also investigated the influence of deposition time on the reflectance spectrum of TiB_2 layer. In order to achieve required selectivity from 1st layer, the target power was kept constant at 75 W, while deposition time was varied from 2 min to 3 min. The

reflectance spectra of TiB_2 film shows a shift in absorption edge towards higher wavelength regime with an increase in deposition time, as shown in Fig. 3(a) and Fig. 3(b). By increasing the deposition time from 2 min to 3 min, the absorptance improves from 0.758 to 0.798, while emittance rises from 0.12 to 0.14, as presented in Fig. 3(c). Further increase in deposition time could also increase the absorptance. However, this could also lead to an increased emittance, which was not desirable for spectrally selective absorber. Therefore, the optimized deposition time was fixed at 3 min and overall optimized parameters for the TiB_2 layer was: TiB_2 target power of 75 W and deposition time of 3 min.

3.1.2. Effect of deposition time and gas flow rate on TiB(N) layer

To enhance the absorptance, TiB(N) was introduced as the second layer on SS/TiB_2 thin film. The condition for solar selectivity can be achieved, when there is a transition from a metallic to dielectric property across the film. It should be stressed that TiB_2 has intrinsic conductivity. The optimized power of TiB_2 target for fabricating TiB_2 layer was 75 W. An increase in TiB_2 target power while depositing TiB(N) layer could affect the graded conductive property of the multilayer thin film. Hence, the TiB_2 target power during preparation of both TiB(N) layer was kept constant at 75 W.

Extensive investigation was performed to understand the effect of deposition time on the selective performance of the coating. A set of samples was prepared by varying the deposition time from 3 to 5 min, keeping the target power of TiB_2 and reactive gas flow of N_2 constant at 75 W and 1 sccm, respectively. In this deposition condition, the growth rate of TiB(N) layer comes out to be ~14.6 nm/min (Supplementary information, Fig. S1(b) and Fig. S2). Fig. 4(a) shows the reflectance spectra from these samples as a function of deposition time. The appearance of reflectance maximum can be observed at 456, 404 and 492 nm for the coatings prepared at 3, 4 and 5 min, respectively. This can be

attributed to the constructive interference phenomenon in the layer interfaces. A shift in the absorptance edge towards longer wavelength can be noticed with an increase in deposition time, which has been depicted in Fig. 4(b). The coating deposited for 5 min exhibits a low reflectance. Fig. 4(c) illustrates the variation of absorptance and emittance with the deposition time. The solar absorptance increased by increasing the deposition time from 3 to 4 min. Further increase of deposition time to 5 min not only enhances the absorptance, but also raises the emittance. In order to satisfy the conflicting requirement of high solar absorptance and low thermal emittance, the optimized deposition time for SS/TiB/TiB(N) coating was found to be 4 min, which corresponds to an absorptance and emittance of 0.920 and 0.16, respectively.

From the experimental data available, it was observed that the reactive gas flow rate on TiB(N) layer also had an effect on the reflectance spectra in Fig. 5. When the N_2 gas flow increases from 1 sccm to 2 sccm, keeping target power and deposition time constant at 75 W and 4 min, respectively, the reflectance in the solar spectrum was found to increase, resulting in poor absorptance. Further increase in reactive N_s gas flow rate for TiB(N) layer could cause "target poisoning". Thus, N_2 gas flow of 1 sccm was kept as optimum for TiB(N) layer.

3.1.3. Effect of nitrogen gas flow rate on Si_3N_4 layer

An antireflection layer was an essential requirement to satisfy the criteria of spectrally selective coating that can achieve maximum absorptance. Therefore, Si_3N_4 layer was introduced on top of TiB_2 and TiB(N) layers. The most influential parameter turned out to be the N_2 flow rate, which was varied within 1 to 2.5 sccm for Si_3N_4 layer, maintaining a constant target power and deposition time of 75 W and 12 min, respectively. The shape of the reflectance spectrum illustrated in Fig. 6(a) changes according to the N_2 flow rate. It is evident from the spectra that a tuneable wavelength-selective reflectance could be

achieved within a narrow range of N_2 flow rate. The coating, deposited at 1 sccm, has high reflectance (> 30% at 448 nm) in the visible region, while the coating deposited at 2.5 sccm exhibits higher reflectance (> 10%) in a wide range of wavelength (ranging from ~ 790-1580 nm). It can be noted that the reflectance of the coating fabricated at 2 sccm was less throughout the entire spectrum. Further, this coating has the lowest reflectance in the spectral range of ~300-1800 nm (< 7%), that makes the coating notably different and superior compared to other two coatings prepared with different gas flow rates. From Fig. 6(b), it is clear that even though the absorptance edge shifts towards longer wavelength for the coatings developed at the gas flow rate of 2.5 sccm, the high reflectance bump around 700-1600 nm leads to a low absorptance. Fig. 6(c) represents the absorptance and emittance values of the coatings deposited at various N_2 gas flow rates. There is a significant increase in the absorptance of the coating prepared at N_2 gas flow rate of 2 sccm, while a drop in emittance was recorded. An increase in the gas flow rate to 2.5 sccm results in a decrease in absorptance, keeping the emittance constant.

If Si_3N_4 film is deposited for much larger time at a constant target power and N_2 gas flow rate, the absorptance will increase inevitably owing to an increase of thickness. Though contribution of thickness in increasing absorption is remarkable, but subsequently it provides a high emittance. Therefore, we deposited Si_3N_4 layer for 12 min at 2 sccm N_2 gas flow rate, so that SS/TiB_2/TiB(N)/Si_3N_4 coating possess a maximum absorptance of 0.964 and minimum emittance of 0.18. All the optimized process parameters for individual layer are summarized in Table 2.

3.2. Spectral selectivity of the coating

The spectral selectivity of TiB_2/TiB(N)/Si_3N_4 coating has been estimated by measuring the reflectance of the coating over a wide wavelength range (0.3-25 μm). The reflectance spectra in solar spectrum (0.3-2.5 μm) and in the infrared spectrum (2.5-25 μm) provide

an evidence to account for the absorption of solar radiation as well as to interpret the heat loss due to thermal emission. Fig. 7(a) illustrates that SS substrate has a very high reflectance (> 60%) over a wide range of wavelength (480-2500 nm). The deposition of TiB_2 layer on SS substrate reduces the reflectance by introducing a reflectance minimum, i.e., absorption edge at 568 nm with a reflectance of ~7%, whereas two reflectance minima appear at 618 and 1380 nm with ~ 5% and 2% reflectance, respectively for TiB(N) layer. The reflectance of TiB_2/TiB(N)/Si_3N_4 coating is <10% for wavelength range of 350-2150 nm. In particular, the reflectance decreases drastically to <2% for 420-485 and 1460-1875 nm. A transition from low to high reflectance can be observed beyond 2300 nm, which is a desired characteristic of spectrally selective absorber. Along with the decreased reflectance in the layer-added coatings, it can be noticed that the absorptance edge also shifts towards longer wavelengths. The absorptance edge with respect to individual layer has been illustrated in Fig. 7(b).

In order to quantify the changes in the reflectance spectra, magnitudes of solar absorptance are very useful as these values provide an idea about absorbed solar energy. In the present work, the findings from reflectance spectra corroborate well with the absorptance values obtained from solar spectrum reflectometer. The absorptance of a bare SS substrate is 0.37-0.38. The absorptance increases drastically to 0.798 for SS/TiB_2, followed by another sharp increment to 0.920 for SS/TiB_2/TiB(N). The incorporation of Si_3N_4 as an antireflection layer enhances the absorptance to 0.964, which is significantly high for a potential spectrally selective absorber coating.

While evaluating the absorptance, it is equally important to focus on the emissive behaviour of the layer-added coating. In that case, one needs to consider Kirchhoff's law of thermal radiation, which demonstrates that the emittance (ε) of a coating equals the absorptance (α) for a constant wavelength. Hence, the reflectance in the infrared region

can represent the emittance characteristics of the coatings on opaque SS substrates. The reflectance spectra for all the coatings appear smooth in Fig. 7(c), with an increasing reflectance towards higher wavelength. A characteristic plateau with high reflectance (~90%) can be noticed beyond 12 μm for all the layer-added coatings as well as SS substrate. One can also observe that the reflectance decreases with an increase in number of layers, indicating an ascending trend of emittance. SS/TiB_2/TiB(N)/Si_3N_4 has the lowest reflectance in the lower wavelength side (2.5-12 μm) among all the coatings and substrate. Hence, the emittance of the SS/TiB_2/TiB(N)/Si_3N_4 coating should be more than other structures, which has been supported by the emittance values measured using emissometer. A polished bare SS substrate has an emittance of 0.12-0.13, whereas SS/TiB_2 coating exhibits an emittance of 0.14. The emittance however increased to 0.16 for SS/TiB_2/TiB(N). Finally, after deposition of final layer, the entire multilayer stack shows an emittance of 0.18. All in all, the investigations on the optical properties reveal that SS/TiB_2/TiB(N)/Si_3N_4 having an absorptance of 0.964 and an emittance of 0.18 satisfies desired criteria to be a potential solar selective absorber coating for photo-thermal application. The absorptance and emittance values of each coating are summarized in Table 3.

3.3. Determination of coating thickness

In order to evaluate the thickness of the optimized coating of TiB_2/TiB(N)/Si_3N_4, deposition process was performed on Si substrate by maintaining the combinations of process parameters for each layer, presented in Table 2. Cross-sectional sample prepared using Focused Ion Beam (FIB) was studied by transmission electron microscopy. The dark field image presented in Fig. 8 shows the coating thickness to be approximately 184 nm with individual layer thicknesses of 58, 56 and 70 nm for TiB_2, TiB(N) and Si_3N_4

layer, respectively. It can also be observed that the coating structure is uniform and crack free.

3.4. Investigation on optical constants

The optical constants of a thin film can be evaluated using spectroscopic ellipsometric data (Krawicz et al., 2012). The amplitude and phase difference between the parallel (p) and perpendicular (s) components of the reflected light with respect to the plane of incidence can be expressed using following equation (Dan et al., 2018):

$$\rho = \frac{r_p}{r_s} = tan\Psi \exp(i\Delta) \qquad (1)$$

where r_p and r_s are the reflection coefficients for p and s components, respectively. Ψ and Δ measure the amplitude ratio and relative phase change between p and s components, respectively.

Fig. 9 represents experimental and model fitted Ψ and Δ data measured at an incidence angles of 65, 70, and 75° using variable-angle spectroscopic ellipsometer in the wavelength range of 200-1000 nm for single layers of TiB_2, TiB(N) and Si_3N_4 deposited on polished SS substrates. The thicknesses of the coatings were around ~ 176, 146, and 73 nm for TiB_2, TiB(N) and Si_3N_4, respectively (Supplementary information, Fig. S1 (a), (b) and (c)). The absence of any interference oscillation in Fig. 9(a-c) reflects the absorbing behaviour of TiB_2 film through interband transition (Liu et al., 2006). In order to extract the optical constants of TiB_2 layer, B-spline (basis spline) function was used to fit the measured Ψ and Δ data, shown in Fig. 9(a-c). The dielectric function of a thin film is related to B-spline function by the following equation (Johs and Hale, 2008; Weber et al., 2010; Weber et al., 2009):

$$S(x) = \sum_{i=1}^{n} C_i B_i^k (x) , \qquad (2)$$

where $S(x)$ denotes the total spline curve, representing the dielectric function of a thin film. C_i are the B-spline coefficients. B-splines are a special set of precise polynomials, which can be defined by the following recurring formula;

$$B_i^0 = \begin{cases} 1, & t_i \le x \le t_{i+1} \\ 0, & otherwise \end{cases}, \qquad (3)$$

$$B_i^k(x) = \left(\frac{x-t_i}{t_{i+k}-t_i}\right) B_i^{k-1}(x) + \left(\frac{t_{i+k+1}-x}{t_{i+k+1}-t_{i+1}}\right) B_{i+1}^{k-1}(x) . \quad (4)$$

The superscript on the function represents the degree, k of the B-spline, and the subscript i denotes the knot locations t_i, which are the connecting points of polynomials.

Fig. 9(d-f) illustrate a typical SE spectrum and fitting curve for the single layer TiB(N) coating, deposited on SS substrate. It is clearly seen that there is a good agreement between experimental data and fitting data. The Cauchy's equation was applied to describe the dispersion of the sample, as expressed in the following (Schmid et al., 2014);

$$n(\lambda) = A + \frac{B}{\lambda^2} + \frac{C}{\lambda^4} . \qquad (5)$$

where, A, B, C are the fitting parameters. A denotes the long wavelength asymptotic refractive index value. B and C influence the slope and amplitude of the refractive index curve, respectively.

The optical response of Si_3N_4 coating, as shown in Fig. 9(g-i), has been explicitly fitted using Tauc-Lorentz model demonstrated by Jellison and Modine (Jellison Jr and Modine, 1996). The model combines the Lorentzian equation with an expression for the imaginary dielectric constant, ε" which has been established by Tauc et al. (Tauc et al., 1966) and expanded by Forouhi and Bloomer (Forouhi and Bloomer, 1986). For a material with optical bandgap (E_g) of $\hbar\omega_g$, ε" can be written as;

$$\varepsilon''(\omega) = \begin{cases} \frac{A\omega_O\Gamma(\omega-\omega_g)^2}{(\omega^2-\omega_O{}^2)^2+\Gamma^2\omega^2}\frac{1}{\omega}, & \omega > \omega_g, \\ 0, & \omega < \omega_g, \end{cases} \qquad (6)$$

In the above equation, A,ω_O, Γ, and ω_g are the amplitude, centre frequency, broadening and band gap frequency, respectively. The real part of the dielectric constant, ε' can be obtained by Kramers–Kronig integration.

Figs. 10(a-c) show the refractive indices, extinction coefficients and absorption coefficients for three layers extracted from the best fitting results. The refractive index profile of TiB_2 in Fig. 10(a) has a maximum and minimum at 281 and 346 nm, respectively and thereafter refractive index increases with wavelength. The extinction coefficient in Fig. 10(b) also has a minimum at 309 nm, followed by a sharp increase in wavelength. The change in optical constants indicates that TiB_2 exhibits metallic property. On the other hand, n and k of TiB(N) layer monotonically decrease with an increase in wavelength. In addition, k value of TiB(N) coating is almost zero in infrared region, whereas k value of Si_3N_4 layer is zero for 200 -1000 nm representing the transparent behaviour. These results demonstrate that Si_3N_4 layer is dielectric in nature, while TiB(N) layer possess an intermediate character, i.e., a transition between the dielectric and metallic behaviour (Meng et al., 2017).

It is well known that the absorption of solar energy depends on the absorption coefficient of a material, which can be represented by;

$$\alpha = \frac{4\pi k}{\lambda} \qquad (7)$$

Fig. 10(c) represents the variation of absorption coefficients with respect to wavelength. It can be observed that TiB_2 has a maximum absorption coefficient, while Si_3N_4 has an absorption coefficient of zero in the entire wavelength range, representing the absorbing and transparent nature of TiB_2 and Si_3N_4, respectively. TiB(N) coating, having an intermediate absorption coefficient, acts as semi-transparent layer in the multi-layer stack.

4. Discussion

In the preceding section, the effect of deposition parameter on the selective performance of $TiB_2/TiB(N)/Si_3N_4$ is described. Along with investigation on parameterizing the fabrication process, efforts should also be made to achieve spectral selectivity and durability. Very few attempts are made to explore evolution of such properties with ultra-high temperature ceramics (UHTCs) that can establish their potentials for photothermal conversion. Investigation on the boride absorber coating was initiated by Randich et al (Randich, 1979; Randich and Allred, 1981). In recent years, a rapid progress on selective property evaluation of these coatings has been attempted. For example, Sani et al. (Sani et al., 2016) systematically established the spectral selective properties of ZrB_2 and TaB_2, synthesised by Self-propagating High-temperature Synthesis (SHS) together with Spark Plasma Sintering (SPS). In a separate study, Sciti et al. (Sciti et al., 2014) investigated structural, compositional, and optical properties of TaB_2 samples to demonstrate their potential as solar selective absorbers. In another study, Sani et al. (Sani et al., 2017) explored promising selective properties of bulk TiB_2 to utilize it as a solar absorber in high temperature concentrating solar power systems due to its good chemical stability, appreciable thermal conductivity (60 $Wm^{-1}k^{-1}$), high hardness (25-32 GPa) and superior mechanical stability (Golla et al., 2015; Mukhopadhyay et al., 2009; Murthy, T.S.R. et al., 2006; Murthy, T.S.R.C. et al., 2006). In the same work, Sani et al. also (Sani et al., 2017) elucidated the better absorption property of TiB_2 compare to other borides (α=0.49 for TiB_2, 0.4 for TaB_2 and 0.47 for ZrB_2). However, it can be noted that the absorptance of bulk TiB_2 is considerably low. In the above backdrop, the present work, for the first time, reports the possibility of achieving high spectral selectivity in a multilayer absorber of $TiB_2/TiB(N)/Si_3N_4$.

The excellent absorptance in a multilayer structure can be achieved by two absorption enhancement mechanisms. The first is intrinsic absorption within the individual layer

which depends on the extinction coefficients of materials. Another mechanism is based on the destructive interference between the reflected rays from the layer interfaces, which gives rise to a very broad as well as strong absorptance in the entire spectrum. It is noteworthy to mention that because of the presence of minimal amount of materials, the interference induced absorbers are most successful in achieving low thermal emittance. A significant improvement can be achieved by continuously grading the optical properties of the absorber layers from a high n, high k material (metallic properties) at the bottom layer to a low n, low k material (dielectric properties) at the top surface (Du et al., 2011; Meng et al., 2017; Selvakumar et al., 2012; Zhang et al., 2017). Further, the sequence of a multilayer selective coating should be substrate/absorber layer/semi-transparent layer/anti-reflector. The deposition of semi-transparent layer is necessary as the absence of this transition layer will lead to an abrupt step in refractive index between absorber and anti-reflector. Even a small amount of grading near the surface can produce a substantial improvement in solar absorptance. The implementation of the inhomogeneity in the metallic properties throughout the stack has been possible only after a careful optimization of the process parameters with a proper adaptation of specific architecture of TiB_2/TiB(N)/Si_3N_4.

In order to explain the gradation in the metallic properties, we have considered different optical responses from these three layers. In pure metals (excluding low temperature region), the electron-phonon interaction is the dominant factor governing electrical conductivity of the material. The electrical conductivity of TiB_2 is 14.4 μΩ cm and hence attractive for preparation of hot-pressed composite materials (Yamada et al., 2003), set up for positron annihilation (Ismail et al., 2015), and copper matrix composites (CMCs) (Zou et al., 2017) and many similar applications. The nature of bonding in TiB_2 is mixed, consisting of ionic, metallic and covalent bonds (Vajeeston and Asokamani).

The delocalised electrons of TiB_2 move in the solid lattice, which leads to good electrical conductivity. Due to relaxation of the delocalised electrons, the solar radiation is absorbed in metallic TiB_2 and acts as main absorbing layer. The electronic transition of TiB_2 is also supported by an increase in absorption co-efficient on the shorter wavelength side, as shown in Fig. 10(c). Since TiB_2 layer is not transparent in NIR, an increase in the target power lead to an increase in the emittance of the coating at 150 W (see Fig. 2(c)). The incorporation of nitrogen in TiB_2 results in a decrease in metallic property of the film. The sharp increase in absorptance after introducing TiB(N) layer can also be attributed to incorporation of nitrogen in TiB_2 matrix. It has been reported that the transmittance of Ti-B-N film increased with nitrogen flow rate (Pierson et al., 2002). In a related account, BN has high optical transparency. The number of B-N bonds continuously increases with N_2 flow rate, which leads to an increase in the transmittance of the film. As a result, the probability of the occurrence of destructive interference increases and SS/TiB_2/TiB(N) coating inherits a high absorptance, as shown in Fig. 4(a). The reflectance of TiB(N) coating, prepared for 5 min is relatively low, compared to the coatings, deposited for 3 and 4 min, respectively, indicating an improved solar absorptance. Considerable difficulty has been experienced in optimizing TiB(N) layer as the film thickness increases with an increase in deposition time, which can be observed from the shifting of absorption edge towards longer wavelength (see Fig. 4(b)) (Liu et al., 2012). As a result, the emittance of the coating tends towards a high value. In order to maintain the emittance of the multilayer stack, the cut-off wavelength for second layer should be no longer than 1.5 μm. Even though the absorptance of the coating fabricated for 4 min is not as high as the coating prepared for 5 min, we have optimized the deposition time of 4 min as that seemed to be the best compromise between high absorptance and low emittance.

The optimization of reactive N_2 gas flow for Si_3N_4 layer is of great relevance to obtain higher selectivity as reflection of incident solar radiation from the front surface of the thin film represents the major optical loss mechanism seriously affecting the photo-thermal conversion efficiency. The Si_3N_4 layer reduces surface reflection by increasing transmission of light. It has been demonstrated by Gang et al. (Xu et al., 2003) that the transmittance of the coating changes with N_2 flow rate due to the change of electronic structure dominated by nitrogen incorporation in the film. While considering the reflectance spectra of individual sample prepared in different gas flow rate (see Fig. 6(a)), the curve around the transition from low to high reflectance becomes steepest for the coating deposited at a N_2 flow rate of 2 sccm and hence represents highest absorptance. A moderately low n value and k = 0 reveal the dielectric behaviour of Si_3N_4 and is therefore suitable as an antireflection layer.

From the perspective of optical selectivity, the main idea of incorporating the anti-reflection layer is to shift the absorption edge towards longer wavelength. In practice, maximum absorptance and minimum emittance are achieved, when the first reflectance minimum occurs at $\lambda \sim 1.6$ μm, leading to a high reflectance for $\lambda > 1.6$ μm, and a high absorptance around $\lambda \sim 0.53$ μm, the peak of solar spectrum (Ritchie and Window, 1977). Taking a closer look at the reflectance spectra in Fig. 7(a), one can clearly see that the absorption edge has moved from 1380 to 1686 nm and reflectance has dropped down drastically around 400-600 nm after introducing Si_3N_4 on top of SS/TiB_2/TiB(N) coating. As a result, the SS/TiB_2/TiB(N)/Si_3N_4 coating possess the signature spectral characteristics of the spectrally selective absorber coating. Also, the successful monitoring and control of the deposition parameters helps us to achieve the required sequences of the refractive indices: $n_{air} > n_{TiB_2} > n_{TiB(N)} > n_{Si_3N_4}$.

The initial investigation by us on the stability of TiB_2/TiB(N)/Si_3N_4 at higher temperature indicates inadequacy of the coating. However, our research provides useful information about the degradation of TiB_2 at nanoscale. While high thermal stability of bulk TiB_2 is widely accepted, we demonstrate, in the present case, that the stability of TiB_2 based thin films, deposited by magnetron sputtering is inadequate. Therefore, TiB_2/TiB(N)/Si_3N_4 in current form needs further improvement for use in CSP systems. The present experimental studies to explore the influence of various deposition parameters on selective performance on TiB_2/TiB(N)/Si_3N_4 coating, however, opens up possibility for further tuning of the multilayer films with graded refractive index profile.

We do have made some efforts to select deposition parameters for the process of sputtering, which are known to affect the optical behaviour of TiB_2/TiB(N)/Si_3N_4. Appropriate sputtering condition and stacking of individual layers allow selective absorption with a minimum heat loss. The experimental results clearly demonstrate the feasibility of preparing boride based thin film by tailoring process parameters. The stability issue that restricts the practical application of the coating may be addressed by encapsulating TiB_2/TiB(N)/Si_3N_4 using multiple anti-reflection layers. Another approach is to insert some additional intermediate layers with different chemical compositions which can restrict the degradation. By combing such specific conditions with strong selective property of boride-based coating, it may be possible to obtain stability of the coating. The realistic technological implementation of the film by employing such strategies can be further elaborated in near future.

5. Conclusions

In this work, novel TiB_2/TiB(N)/Si_3N_4 coating has been fabricated by DC and RF magnetron sputtering. An optimization procedure was carried out to unveil the influence of sputtering conditions on the spectral selective behaviour of the coating. The proposed

approach was utilized to achieve maximum absorptance of 0.964 in the solar spectrum (0.3-2.5 μm) and minimum emittance of 0.18 at 82 °C in the infrared regime (2.5-25 μm). Based on the experimental results, various properties of the coating, in particular optical properties have been analysed extensively. The major conclusions are,

a) The appropriate choice of sputtering parameters determines the position of absorption edge i.e. the transition point between low and high values of reflectance. For TiB_2 and TiB(N) layers, thermal emittance increased rapidly when there is a displacement of the absorption edge towards longer wavelength.
b) The increase in deposition time is associated with increasing amount of film material, which showed an adverse effect on the thermal emittance of SS/TiB_2/TiB(N) coating.
c) The efficacy of Si_3N_4 as antireflection layer to obtain optimum spectral selectivity has been established.
d) Our results demonstrate that the gradation in refractive indices and metallic properties among different layers can exert a strong influence on the spectral selectivity. The mismatch in the refractive indices helps the destructive interference conditions to match and thus, the absorptance of the system increases.
e) General concepts on oxidation resistance of TiB_2 is not manifested in nano scale which is evident from thermal and environmental instability of TiB_2/TiB(N)/Si_3N_4 system. However, the experimental studies to explore the influence of various deposition parameters on selective performance on graded TiB_2/TiB(N)/Si_3N_4 coating could be extended to other potential multilayer absorber systems.

Acknowledgments

The authors thank Dr. Altaf Basha and Mr. G. Srinivas for microscopy and UV-Vis-NIR measurements. Research at CSIR-NAL is partially supported by Department of

Science and Technology, New Delhi (U-1-144). This paper is based upon work supported in part under the US-India Partnership to Advance Clean Energy-Research (PACE-R) for the Solar Energy Research Institute for India and the United States (SERIIUS), funded jointly by the U.S. Department of Energy (Office of Science, Office of Basic Energy Sciences, and Energy Efficiency and Renewable Energy, Solar Energy Technology Program, under Subcontract DE-AC36-08GO28308 to the National Renewable Energy Laboratory, Golden, Colorado) and the Government of India, through the Department of Science and Technology under Subcontract IUSSTF/JCERDC-SERIIUS/2012 dated 22nd Nov. 2012. Atasi Dan acknowledges DST for providing INSPIRE scholarship.

Figure Captions

Fig. 1. Architecture of SS/TiB_2/TiB(N)/Si_3N_4 multilayer coating.

Fig. 2. (a) Variation of reflectance spectra of SS/TiB_2 at different target powers, (b) absorption edge as a function of target power, (c) change in absorptance and emittance with target power for SS/TiB_2 coating. The best combination of absorptance and emittance can be obtained at a TiB_2 target power of 75 W.

Fig. 3. (a) Reflectance spectra of SS/TiB_2 at different deposition time, (b) shift in absorption edge with deposition time, (c) variation in absorptance and emittance with deposition time for SS/TiB_2 coating. The best combination of absorptance and emittance can be obtained at a deposition time of 3 min.

Fig. 4. (a) Reflectance spectra of TiB_2/TiB(N) coating at various deposition times, (b) displacement of absorption edge with increase in deposition time, (c) evolution of absorptance and emittance over deposition time for SS/TiB_2/TiB(N) coating. The optimized deposition time is 4 min.

Fig. 5. Difference in reflectance spectra of TiB_2/TiB(N) thin film, prepared using 1 and 2 sccm reactive N_2 gas flow rate. The target power and deposition time was 75 W and 4 min, respectively.

Fig. 6. (a) Effect of N_2 flow rates on the reflectance spectra, (b) shift of absorption edge as a function of N_2 flow rate, and (c) dependence of absorptance and emittance on N_2 gas flow rates for TiB_2/TiB(N)/Si_3N_4 coating deposited on SS substrate. The coating possesses highest selectivity at N_2 flow rate of 2 sccm.

Fig. 7. (a) Reflectance properties of successive layers deposited on stainless steel substrates in solar wavelength range, (b) the shift in absorption edge with increased number of layers, (c) the reflectance spectra of layer-added coatings in infrared regime.

Fig. 8. Cross-sectional TEM dark field image of $TiB_2/TiB(N)/Si_3N_4$ coating deposited on Si substrate. The multilayer coating is comprised of three distinct layers.

Fig. 9. Spectroscopic ellipsometry data of (a-c) TiB_2, (d-f) TiB(N), and (g-i) Si_3N_4 single layer coatings fabricated on SS substrates. The left, middle and right panel shows experimental (open symbols) and fitted (solid line) ψ and Δ data collected at an incidence angle of 65, 70, and 75°, respectively.

Fig. 10. (a) Refractive index (n), (b) extinction coefficient (k), and (c) absorption coefficient, obtained from the best fitting results of ellipsometry data for single layer TiB_2, TiB(N), and Si_3N_4 coating deposited on SS substrates.

List of Tables

Table 1: Sputtering conditions during $TiB_2/TiB(N)/Si_3N_4$ deposition.

Table 2: Optimized sputtering parameters for the deposition of $TiB_2/TiB(N)/Si_3N_4$ coating on stainless steel substrate.

Table 3: Absorptance (α) and emittance (ε) of layer-added coatings.

References

Barshilia, H.C., Selvakumar, N., Rajam, K.S., Rao, D.V.S., Muraleedharan, K., Biswas, A., 2006. TiAlN/TiAlON/Si_3N_4 tandem absorber for high temperature solar selective applications. Applied physics letters 89(19), 191909-191909.
Chen, Z., Boström, T., 2016. Electrophoretically deposited carbon nanotube spectrally selective solar absorbers. Solar Energy Materials and Solar Cells 144, 678-683.
Dan, A., Barshilia, H.C., Chattopadhyay, K., Basu, B., 2017. Solar energy absorption mediated by surface plasma polaritons in spectrally selective dielectric-metal-dielectric coatings: A critical review. Renewable and Sustainable Energy Reviews 79, 1050-1077.
Dan, A., Biswas, A., Sarkar, P., Kashyap, S., Chattopadhyay, K., Barshilia, H.C., Basu, B., 2018. Enhancing spectrally selective response of W/WAlN/WAlON/Al_2O_3 –based nanostructured multilayer absorber coating through graded optical constants. Solar Energy Materials and Solar Cells 176, 157-166.
Dan, A., Chattopadhyay, K., Barshilia, H.C., Basu, B., 2016a. Angular solar absorptance and thermal stability of W/WAlN/WAlON/Al_2O_3-based solar selective absorber coating. Applied Thermal Engineering 109, 997-1002.
Dan, A., Chattopadhyay, K., Barshilia, H.C., Basu, B., 2016b. Colored selective absorber coating with excellent durability. Thin Solid Films 620, 17-22.
Dan, A., Chattopadhyay, K., Barshilia, H.C., Basu, B., 2016c. Thermal stability of WAlN/WAlON/Al_2O_3 -based solar selective absorber coating. MRS Advances CJO2016., doi:10.1557/adv.2016.1388.

.
Du, M., Hao, L., Mi, J., Lv, F., Liu, X., Jiang, L., Wang, S., 2011. Optimization design of $Ti_{0.5}Al_{0.5}N/Ti_{0.25}Al_{0.75}N$/AlN coating used for solar selective applications. Solar Energy Materials and Solar Cells 95(4), 1193-1196.
Duffie, J.A., Beckman, W.A., 2013. Solar engineering of thermal processes. John Wiley & Sons.
Feng, J., Zhang, S., Lu, Y., Yu, H., Kang, L., Wang, X., Liu, Z., Ding, H., Tian, Y., Ouyang, J., 2015. The spectral selective absorbing characteristics and thermal stability of SS/TiAlN/TiAlSiN/Si_3N_4 tandem absorber prepared by magnetron sputtering. Solar Energy 111, 350-356.
Forouhi, A.R., Bloomer, I., 1986. Optical dispersion relations for amorphous semiconductors and amorphous dielectrics. Physical review B 34(10), 7018.
Gao, X.-H., Wang, C.-B., Guo, Z.-M., Geng, Q.-F., Theiss, W., Liu, G., 2016. Structure, optical properties and thermal stability of Al_2O_3-WC nanocomposite ceramic spectrally selective solar absorbers. Optical Materials 58, 219-225.
Gauché, P., Rudman, J., Mabaso, M., Landman, W.A., von Backström, T.W., Brent, A.C., 2017. System value and progress of CSP. Solar Energy 152, 106-139.
Golla, B.R., Bhandari, T., Mukhopadhyay, A., Basu, B., 2015. Titanium diboride. Ultra-High Temperature Ceramics: Materials for Extreme Environment Applications, 316-360.
Granqvist, C.G., Niklasson, G.A., 2018. Solar energy materials for thermal applications: A primer. Solar Energy Materials and Solar Cells 180, 213-226.
Gupta, M.C., Ungaro, C., Foley, J.J., Gray, S.K., 2018. Optical nanostructures design, fabrication, and applications for solar/thermal energy conversion. Solar Energy 165, 100-114.
Ismail, A.M., Mahmoud, K.R., Abd-El Salam, M.H., 2015. Electrical conductivity and positron annihilation characteristics of ternary silicone rubber/carbon black/TiB_2 nanocomposites. Polymer Testing 48, 37-43.
Jellison Jr, G.E., Modine, F.A., 1996. Parameterization of the optical functions of amorphous materials in the interband region. Applied Physics Letters 69(3), 371-373.

Jeong, D., Lee, J., Hong, H., Choi, D., Cho, J.-W., Kim, S.-K., Nam, Y., 2017. Absorption mechanism and performance characterization of CuO nanostructured absorbers. Solar Energy Materials and Solar Cells 169, 270-279.
Johs, B., Hale, J.S., 2008. Dielectric function representation by B-splines. physica status solidi (a) 205(4), 715-719.
Kalogirou, S.A., Karellas, S., Braimakis, K., Stanciu, C., Badescu, V., 2016. Exergy analysis of solar thermal collectors and processes. Progress in Energy and Combustion Science 56, 106-137.
Kim, J., Park, J., Hong, J.H., Choi, S.J., Kang, G.H., Yu, G.J., Kim, N.S., Song, H.-e., 2013. Double antireflection coating layer with silicon nitride and silicon oxide for crystalline silicon solar cell. Journal of Electroceramics 30(1-2), 41-45.
Klochko, N.P., Klepikova, K.S., Tyukhov, II, Myagchenko, Y.O., Melnychuk, E.E., Kopach, V.R., Khrypunov, G.S., Lyubov, V.M., Kopach, A.V., Starikov, V.V., 2015. Zinc oxide–nickel cermet selective coatings obtained by sequential electrodeposition. Solar Energy 117, 1-9.
Krawicz, A., Palazzo, J., Wang, G.-C., Dinolfo, P.H., 2012. Layer-by-layer assembly of Zn (II) and Ni (II) 5, 10, 15, 20-tetra (4-ethynylphenyl) porphyrin multilayers on Au using copper catalyzed azide-alkyne cycloaddition. RSC Advances 2(19), 7513-7522.
Liu, Y., Wang, C., Xue, Y., 2012. The spectral properties and thermal stability of NbTiON solar selective absorbing coating. Solar energy materials and solar cells 96, 131-136.
Liu, Y.C., Hsieh, J.H., Tung, S.K., 2006. Extraction of optical constants of zinc oxide thin films by ellipsometry with various models. Thin Solid Films 510(1), 32-38.
Meng, J.-p., Liu, X.-p., Fu, Z.-q., Zhang, K., 2017. Optical design of $Cu/Zr_{0.2}AlN_{0.8}/ZrN/AlN/ZrN/AlN/Al_{34}O_{62}N_4$ solar selective absorbing coatings. Solar Energy 146, 430-435.
Mukhopadhyay, A., Raju, G.B., Basu, B., Suri, A.K., 2009. Correlation between phase evolution, mechanical properties and instrumented indentation response of TiB_2-based ceramics. Journal of the European Ceramic Society 29(3), 505-516.
Murthy, T.S.R., Basu, B., Balasubramaniam, R., Suri, A.K., Subramanian, C., Fotedar, R.K., 2006. Processing and Properties of TiB_2 with $MoSi_2$ Sinter-additive: A First Report. Journal of the American Ceramic Society 89(1), 131-138.
Murthy, T.S.R.C., Basu, B., Srivastava, A., Balasubramaniam, R., Suri, A.K., 2006. Tribological properties of TiB_2 and TiB_2–$MoSi_2$ ceramic composites. Journal of the European Ceramic Society 26(7), 1293-1300.
Pierson, J.F., Tomasella, E., Bauer, P., 2002. Reactively sputtered Ti–B–N nanocomposite films: correlation between structure and optical properties. Thin Solid Films 408(1), 26-32.
Randich, E., 1979. Chemical vapor deposited borides of the form (Ti, Zr)B_2 and (Ta, Ti)B_2. Thin Solid Films 63(2), 309-313.
Randich, E., Allred, D.D., 1981. Chemically vapor-deposited ZrB_2 as a selective solar absorber. Thin Solid Films 83(4), 393-398.
Ritchie, I.T., Window, B., 1977. Applications of thin graded-index films to solar absorbers. Applied optics 16(5), 1438-1443.
Rodríguez-Palomo, A., Céspedes, E., Hernández-Pinilla, D., Prieto, C., 2018. High-temperature air-stable solar selective coating based on $MoSi_2$–Si_3N_4 composite. Solar Energy Materials and Solar Cells 174, 50-55.
Saleh, A., Mosa, M., 2014. Optimization study of a single-effect water–lithium bromide absorption refrigeration system powered by flat-plate collector in hot regions. Energy Conversion and Management 87, 29-36.
Sani, E., Mercatelli, L., Meucci, M., Balbo, A., Musa, C., Licheri, R., Orrù, R., Cao, G., 2016. Optical properties of dense zirconium and tantalum diborides for solar thermal absorbers. Renewable Energy 91, 340-346.
Sani, E., Meucci, M., Mercatelli, L., Balbo, A., Musa, C., Licheri, R., Orrù, R., Cao, G., 2017. Titanium diboride ceramics for solar thermal absorbers. Solar Energy Materials and Solar Cells 169, 313-319.

Schmid, M., Andrae, P., Manley, P., 2014. Plasmonic and photonic scattering and near fields of nanoparticles. Nanoscale research letters 9(1), 50.
Sciti, D., Silvestroni, L., Sans, J.-L., Mercatelli, L., Meucci, M., Sani, E., 2014. Tantalum diboride-based ceramics for bulk solar absorbers. Solar Energy Materials and Solar Cells 130, 208-216.
Selvakumar, N., Barshilia, H.C., 2012. Review of physical vapor deposited (PVD) spectrally selective coatings for mid-and high-temperature solar thermal applications. Solar energy materials and solar cells 98, 1-23.
Selvakumar, N., Barshilia, H.C., Rajam, K.S., Biswas, A., 2010. Structure, optical properties and thermal stability of pulsed sputter deposited high temperature HfO_x/Mo/HfO_2 solar selective absorbers. Solar Energy Materials and Solar Cells 94(8), 1412-1420.
Selvakumar, N., Krupanidhi, S.B., Barshilia, H.C., 2014. Carbon Nanotube-Based Tandem Absorber with Tunable Spectral Selectivity: Transition from Near-Perfect Blackbody Absorber to Solar Selective Absorber. Advanced Materials 26(16), 2552-2557.
Selvakumar, N., Manikandanath, N.T., Biswas, A., Barshilia, H.C., 2012. Design and fabrication of highly thermally stable HfMoN/HfON/Al_2O_3 tandem absorber for solar thermal power generation applications. Solar Energy Materials and Solar Cells 102, 86-92.
Soum-Glaude, A., Le Gal, A., Bichotte, M., Escape, C., Dubost, L., 2017. Optical characterization of $TiAlN_x$/$TiAlN_y$/Al_2O_3 tandem solar selective absorber coatings. Solar Energy Materials and Solar Cells 170, 254-262.
Tauc, J., Grigorovici, R., Vancu, A., 1966. Optical properties and electronic structure of amorphous germanium. physica status solidi (b) 15(2), 627-637.
Thirugnanasambandam, M., Iniyan, S., Goic, R., 2010. A review of solar thermal technologies. Renewable and sustainable energy reviews 14(1), 312-322.
Usmani, B., Dixit, A., 2016. Spectrally selective response of ZrO_x/ZrC–ZrN/Zr absorber–reflector tandem structures on stainless steel and copper substrates for high temperature solar thermal applications. Solar Energy 134, 353-365.
Vajeeston, T.P., Asokamani, R., The electronic structure and ground state properties of Ti_2B, TiB and TiB_2.
Valleti, K., Krishna, D.M., Joshi, S.V., 2014. Functional multi-layer nitride coatings for high temperature solar selective applications. Solar Energy Materials and Solar Cells 121, 14-21.
Wallner, G.M., Resch, K., Hausner, R., 2008. Property and performance requirements for thermotropic layers to prevent overheating in an all polymeric flat-plate collector. Solar Energy Materials and Solar Cells 92(6), 614-620.
Weber, J.W., Calado, V.E., Van De Sanden, M.C.M., 2010. Optical constants of graphene measured by spectroscopic ellipsometry. Applied Physics Letters 97(9), 091904.
Weber, J.W., Hansen, T.A.R., Van de Sanden, M.C.M., Engeln, R., 2009. B-spline parametrization of the dielectric function applied to spectroscopic ellipsometry on amorphous carbon. Journal of Applied Physics 106(12), 123503.
Xu, G., Jin, P., Tazawa, M., Yoshimura, K., 2003. Optical investigation of silicon nitride thin films deposited by rf magnetron sputtering. Thin Solid Films 425(1), 196-202.
Yamada, S., Hirao, K., Yamauchi, Y., Kanzaki, S., 2003. High strength B_4C–TiB_2 composites fabricated by reaction hot-pressing. Journal of the European Ceramic Society 23(7), 1123-1130.
Zhang, J., Chen, T.P., Liu, Y.C., Liu, Z., Yang, H.Y., 2017. Modeling of a selective solar absorber thin film structure based on double TiN_xO_y layers for concentrated solar power applications. Solar Energy 142, 33-38.
Zou, C., Chen, Z., Kang, H., Wang, W., Li, R., Li, T., Wang, T., 2017. Study of enhanced dry sliding wear behavior and mechanical properties of Cu-TiB_2 composites fabricated by in situ casting process. Wear 392, 118-125.
Zou, C., Huang, L., Wang, J., Xue, S., 2015. Effects of antireflection layers on the optical and thermal stability properties of a spectrally selective CrAlN–CrAlON based tandem absorber. Solar energy materials and solar cells 137, 243-252.

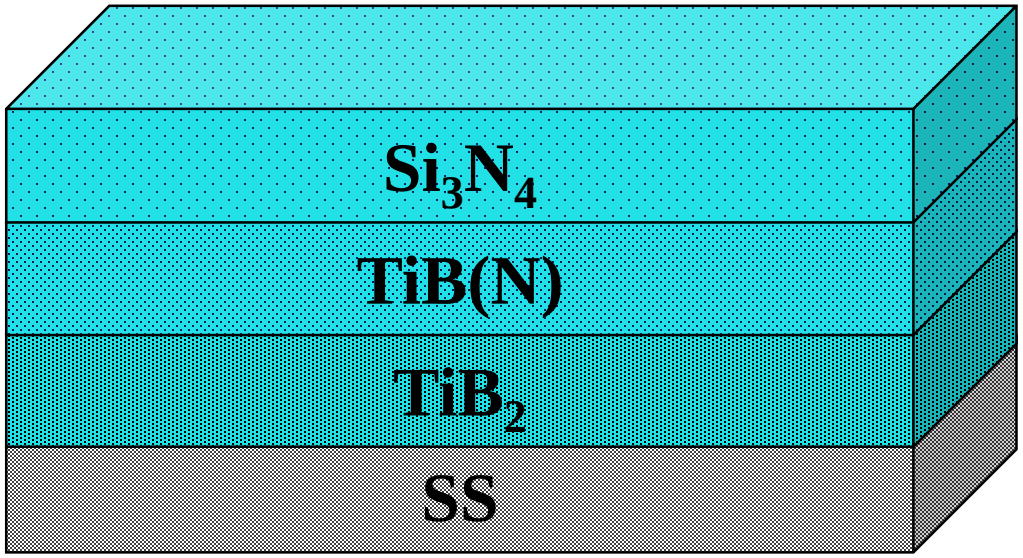

Fig. 1. Architecture of SS/TiB_2/TiB(N)/Si_3N_4 multilayer coating.

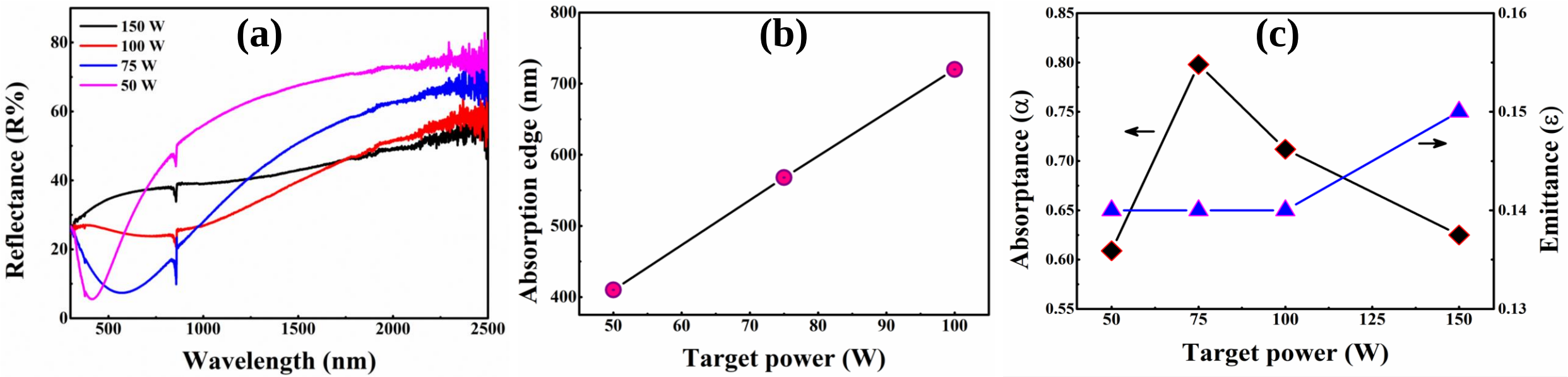

Fig. 2. (a) Variation of reflectance spectra of SS/TiB_2 at different target powers, (b) absorption edge as a function of target power, (c) change in absorptance and emittance with target power for SS/TiB_2 coating. The best combination of absorptance and emittance can be obtained at a TiB_2 target power of 75 W.

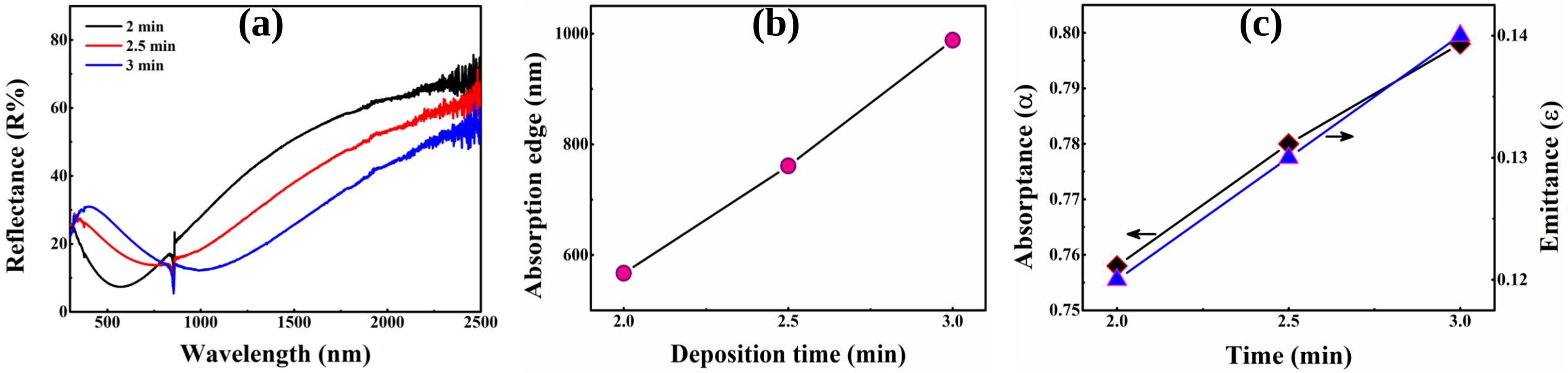

Fig. 3. (a) Reflectance spectra of SS/TiB_2 at different deposition time, (b) shift in absorption edge with deposition time, (c) variation in absorptance and emittance with deposition time for SS/TiB_2 coating. The best combination of absorptance and emittance can be obtained at a deposition time of 3 min.

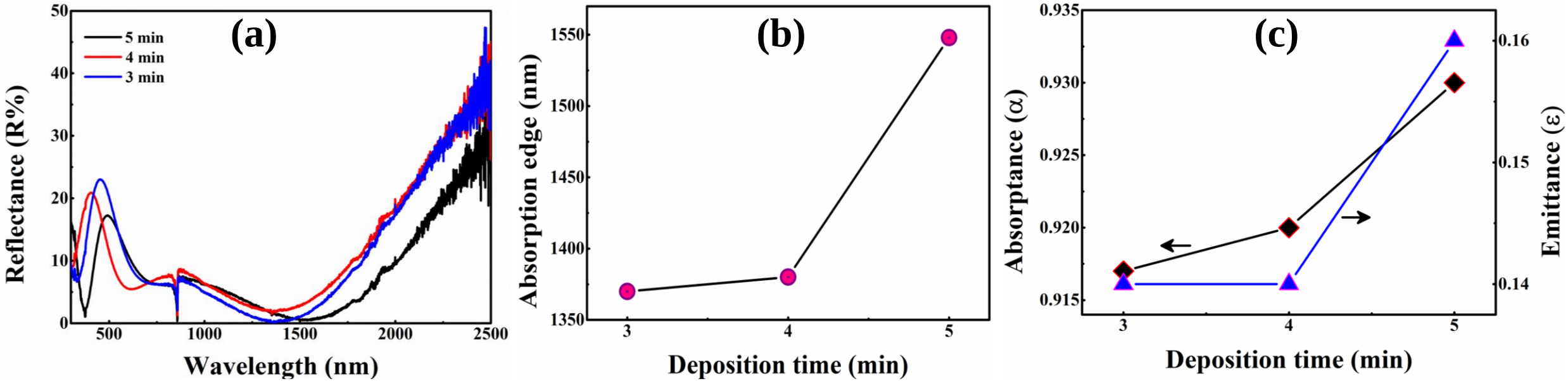

Fig. 4. (a) Reflectance spectra of TiB_2/TiB(N) coating at various deposition times, (b) displacement of absorption edge with increase in deposition time, (c) evolution of absorptance and emittance over deposition time for SS/TiB_2/TiB(N) coating. The optimized deposition time is 4 min.

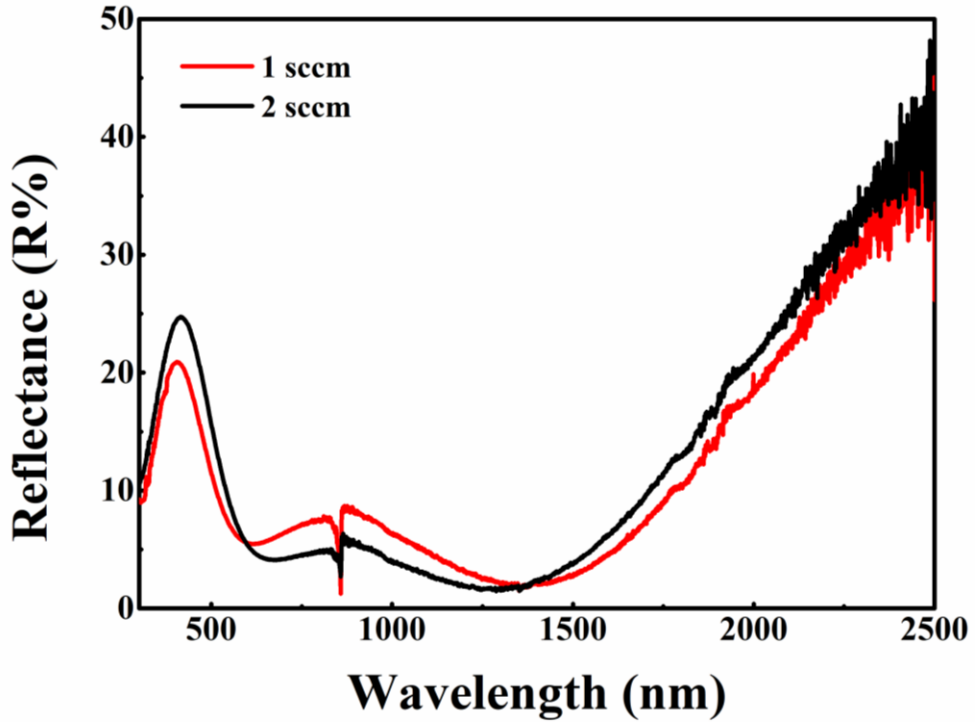

Fig. 5. Difference in reflectance spectra of TiB_2/TiB(N) thin film, prepared using 1 and 2 sccm reactive N_2 gas flow rate. The target power and deposition time was 75 W and 4 min, respectively.

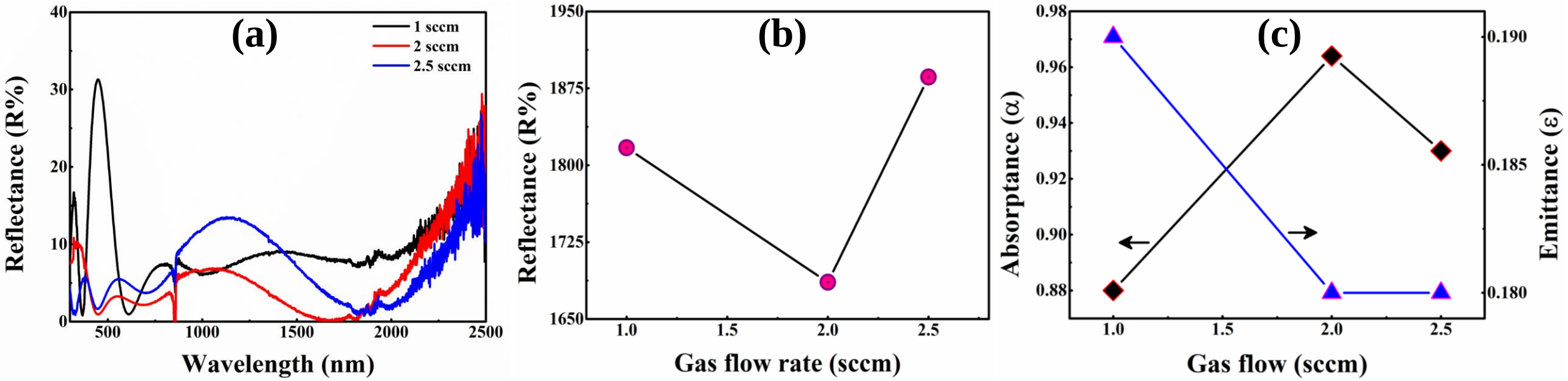

Fig. 6. (a) Effect of N_2 flow rates on the reflectance spectra, (b) shift of absorption edge as a function of N_2 flow rate, and (c) dependence of absorptance and emittance on N_2 gas flow rates for $TiB_2/TiB(N)/Si_3N_4$ coating deposited on SS substrate. The coating posseses highest selectivity at N_2 flow rate of 2 sccm.

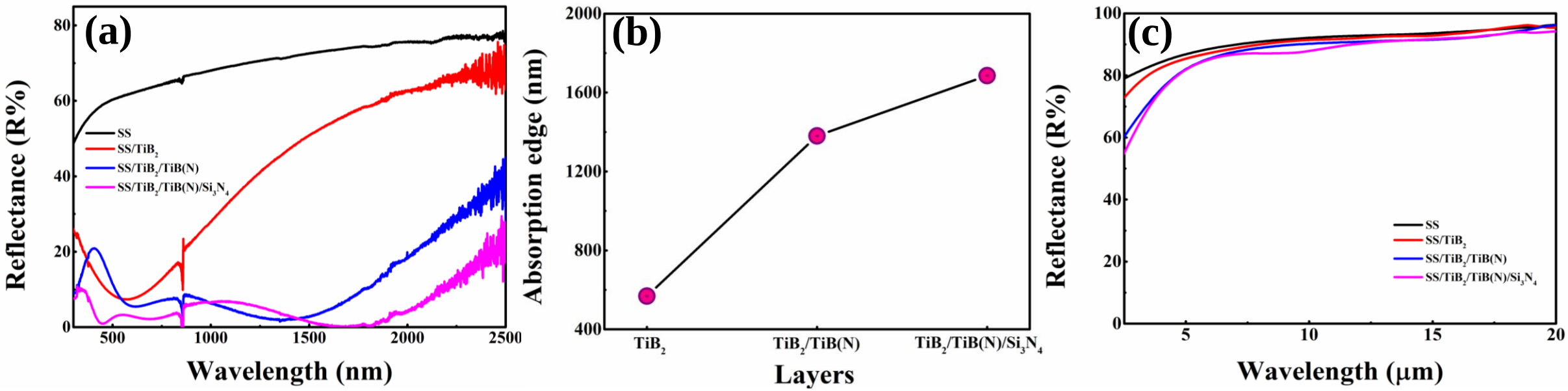

Fig. 7. (a) Reflectance properties of successive layers deposited on stainless steel substrates in solar wavelength range, (b) the shift in absorption edge with increased number of layers, (c) the reflectance spectra of layer-added coatings in infrared regime.

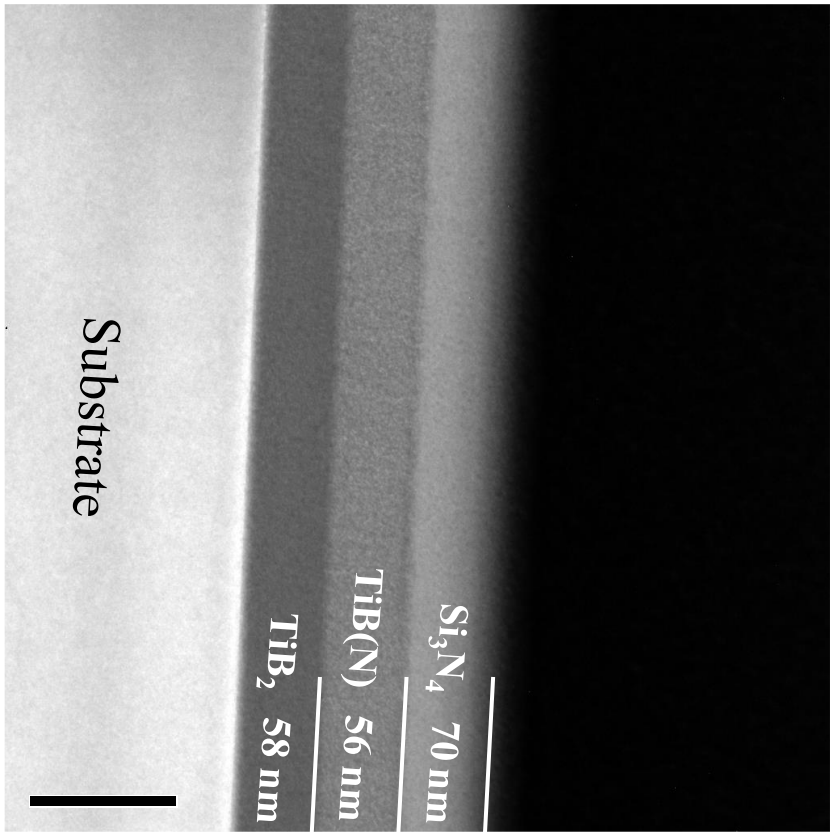

Fig. 8. Cross-sectional TEM dark field image of TiB_2/TiB(N)/Si_3N_4 coating deposited on Si substrate. The multilayer coating is comprised of three distinct layers.

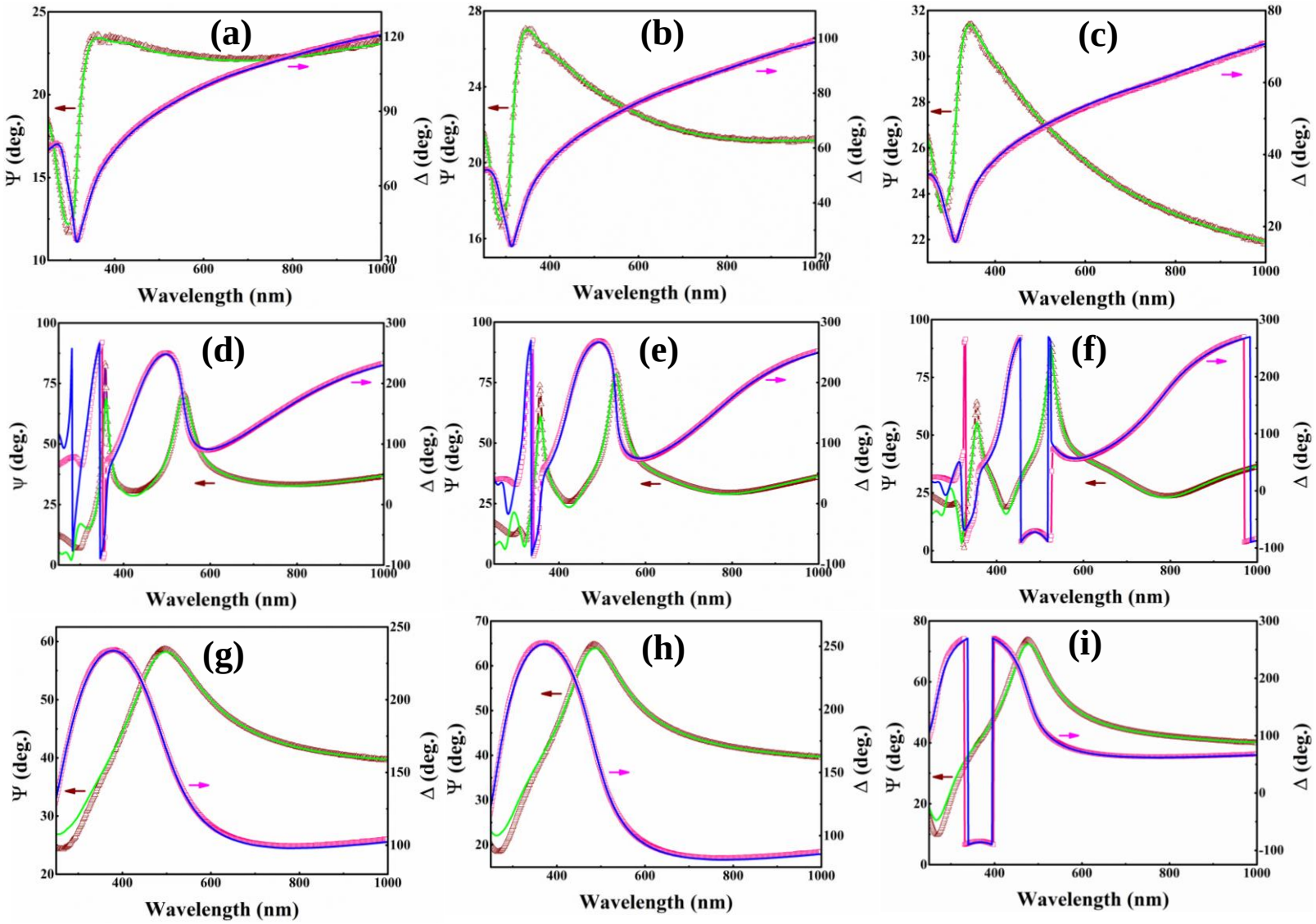

Fig. 9. Spectroscopic ellipsometry data of (a-c) TiB_2, (d-f) TiB(N), and (g-i) Si_3N_4 single layer coatings fabricated on SS substrates. The left, middle and right panel shows experimental (open symbols) and fitted (solid line) ψ and Δ data collected at an incidence angle of 65, 70, and 75°, respectively.

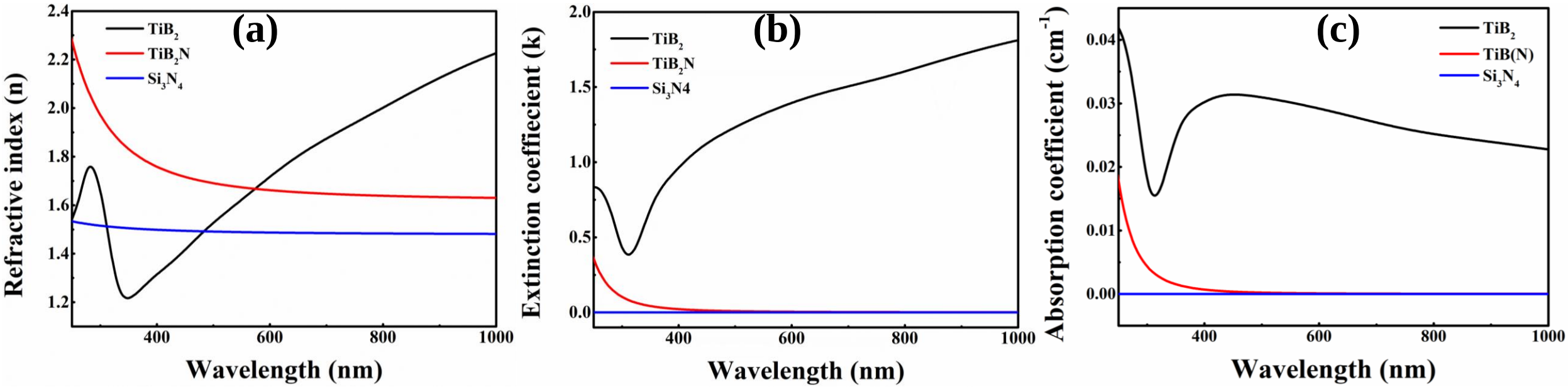

Fig. 10. (a) Refractive index (n), (b) extinction coefficient (k), and (c) absorption coefficient, obtained from the best fitting results of ellipsometry data for single layer TiB_2, TiB(N), and Si_3N_4 coating deposited on SS substrates.

Table 1: Sputtering conditions during TiB_2/TiB(N)/Si_3N_4 deposition.

Parameter	Condition
System	Balanced magnetron sputtering
Target	TiB_2 and Si
Power supply	Pulsed DC and RF
Substrate	Stainless steel (SS)
Substrate temperature	Room temperature
Target-substrate distance	5 cm
Base pressure	5×10^{-4} Pa
Sputtering gas	Ar
Reactive gas	N_2
Target power	Varying
Reactive gas flow rate	Varying
Deposition time	Varying

Table 2: Optimized sputtering parameters for the deposition of TiB_2/TiB(N)/Si_3N_4 coating on stainless steel substrate.

Layer	**Gas flow rate (sccm)**		**Target power (W)**	**Deposition time (min)**
	Ar	**N_2**		
TiB_2	20	-	75	3
TiB(N)	20	1	75	4
Si_3N_4	20	2	75	12

Table 3: Absorptance (α) and emittance (ε) of layer-added coatings.

Sample	**Absorptance (α)**	**Emittance (ε)**
SS	0.37-0.38	0.12-0.13
SS/TiB_2	0.798	0.14
SS/TiB_2/TiB(N)	0.920	0.16
SS/TiB_2/TiB(N)/Si_3N_4	0.964	0.18